RSC Advances

ROYAL SOCIETY OF CHEMISTRY

www.rsc.org/advances

RSC Advances

RSCPublishing

ARTICLE

The Role of Ethynylene Bond on the Optical and Electronic Properties of Diketopyrrolopyrrole Copolymers

Cite this: DOI: 10.1039/x0xx00000x

Received ooth January 2014,
Accepted ooth January 2014

DOI: 10.1039/x0xx00000x

www.rsc.org/

Pichaya Pattanasattayavong,[a] Maria Sygletou,[b] Emmanuel Kymakis,[c] Emmanuel Stratakis,[b] Feng Yan,[d] Vasilis G. Gregoriou,[e,f] Thomas D. Anthopoulos,[a] Christos L. Chochos[f*]

It is presented that the introduction of an alkyne linkage could be an important tool for fine-tuning the electronic and optoelectronic properties of certain donor-acceptor (D-A) conjugated polymers. Extensive optoelectronic studies in an alternating copolymer consisting of diketopyrrolopyrrole (DPP) and ethynylene linkage (TDPPTTB) and comparison over its fully cyclic DPP analogues, such as phenyl (TDPPTP) and thiophene (TDPPTT) rings reveals the role of ethynylene moiety when it is introduced into the polymer backbone. Ethynylene moiety is decreasing the donor character of thiophenes that flank the DPP therefore the highest occupied molecular orbital (HOMO) level of TDPPTTB is situated between the HOMO levels of the TDPPTP and TDPPTT. The optical band gap (E_g^{opt}) of TDPPTTB is fixed between the E_g^{opt} of TDPPTT and TDPPTP with a significant blue-shift in its absorption maximum. Furthermore, detailed studies on the electronic properties of TDPPTTB has been performed in Field Effect Transistors (FETs) using various dielectric materials. Transistors based on TDPPTTB films annealed at 120 °C show ambipolar behaviour, similar to TDPPTP and TDPPTT, with carrier mobilities of 0.03 cm^2 V^{-1} s^{-1} for holes and 0.02 cm^2 V^{-1} s^{-1} for electrons.

Introduction

Polymeric semiconductors are materials where unique optical and electronic properties often originate from a tailored chemical structure. This allows for synthesizing conjugated macromolecules with predefined functionalities for organic electronics such as organic photovoltaics (OPVs),[1] organic field-effect transistors (OFETs),[2] light-emitting diodes (LEDs),[3] and electrochromics.[4] During the past few decades a vast number of conjugated polymers has been developed and various chemical modifications are used to engineer and optimize the physical and optoelectronic properties that suit their specific purpose.[5-7]

Modulation of molecular energy levels is one of the most important topics in molecular design of organic semiconducting materials. For many applications, such as OLEDs and photovoltaics, the value of the HOMO-LUMO gap is critical to an optimized device because it determines the colour of the emitted light in the LED or the effectiveness with which solar radiation is absorbed in photovoltaic devices.[8] However, the control of the HOMO and LUMO energy levels is not a very simple process. Common tools that are employed to fine tune the band gap and energy level alignment of conjugated polymers are the donor-acceptor (D-A) approach and the quinoid structure.[9] Despite the fact that the D-A approach is commonly used for the synthesis of a plethora of new low band gap (LBG) conjugated polymers, many issues remain to be addressed for understanding how their optoelectronic properties are fine-tuned, including the relative strength, the placement, and the ratio of the donor and acceptor moieties in the polymer backbone.[5]

Diketopyrrolopyrrole (DPP) based polymers are currently displaying some of the highest mobilities in field effect transistors (FETs) and PCE in OPVs.[10] The potential of DPP-containing polymers as semiconductor materials for OFETs was presented in 2005.[11] Two of the most extensively studied DPP-based copolymers consisting of either a thiophene[12] or phenyl[13] ring next to the thiophene-diketopyrrolopyrrole-thiophene (TDPPT) segment are presented in Scheme 1. TDPPTT and TDPPTP copolymers exhibit remarkably high hole mobilities up to 0.3 cm^2 V^{-1} s^{-1} and PCEs above 7.0%.[14,15] Very recently, *Janssen et al.* presented the synthesis of regular alternating DPP-based terpolymers containing both thiophene and phenyl rings in the polymer backbone, in an attempt to optimize their optoelectronic properties.[16] Other co-monomers that have also been used are bithiophene,[17] thieno[3,2-*b*]thiophene,[18] furan,[19] selenophene,[20] naphthalene,[21] vinylene,[22] benzodithiophene[23] and dithienothiophene[24] (Scheme 1).

Scheme 1

In this work, ethynylene bond is proposed and extensively explored as another chemical building block to modify the

optoelectronic properties in DPP-based copolymers. The synthesis of an alternating copolymer comprising of the TDPPT segment and ethynylene unit (TDPPTTB; Scheme 1) is presented. Moreover, a direct comparison between the high performance TDPPTT and TDPPTP copolymers and the newly synthesized TDPPTTB will be performed in order to understand the relative strength (weak, intermediate, strong) of the ethynylene bond as compared to the thiophene and phenyl rings and how this affects the optoelectronic properties of DPP copolymers.

Results and discussions

Design and synthesis

The need of fine tuning the optoelectronic properties (absorption characteristics, optical band gap, HOMO and LUMO levels) of conjugated polymers and especially those consisting of the DPP moiety has led to the study of various monomers such as phenyl, thiophene, furan, selenophene, bithiophene, thieno[3,2-*b*]thiophene, naphthalene, benzodithiophene, dithienothiophene, vinylene, etc.. Herein, ethynylene which is the less explored building block in the different families of conjugated polymers will be examined as alternative comonomer in DPP-type copolymers. Theoretical calculations performed on model compounds consisting of TDPPT unit and phenyl, thiophene, and ethynylene demonstrate that the introduction of the ethynylene bond minimizes the dihedral angles (Fig. 1), increasing the planarity of the repeating unit as compared to phenyl and thiophene rings.

Figure 1

TDPPTTB was synthesized by Stille aromatic cross-coupling polymerization[25] using tetrakis(triphenylphosphine)palladium (0) [$Pd(PPh_3)_4$] as the catalyst in toluene solution between the 3,6-bis(5-bromothiophen-2-yl)-2,5-bis(2-hexyldecyl)pyrrolo[3, 4-*c*]pyrrole-1,4(2*H*,5*H*)-dione and the 1,2-bis(trimethylstannyl) ethyne (Scheme 2). The polymerization reaction was performed at 110 ^{o}C under argon atmosphere for 12 h. After purification using Soxhlet extraction, the chloroform-soluble fraction of the TDPPTTB exhibits molecular weight of M_n = 20000 g/mol (PDI = 2.0) as measured by gel permeation chromatography (GPC) on monodisperse polystyrene standards utilizing chloroform as the eluent. The polymer exhibits very good solubility in chlorinated solvents.

Scheme 2

Optical properties

The UV-Vis absorption spectra of TDPPTTB in chloroform solution and as thin film are presented in Fig. 2. Two absorption bands can be observed in solution, a feature which is commonly observed for alternating D-A copolymers. A major peak at 710 nm due to the intramolecular D-A charge transfer character and a low intensity high energy band at 420 nm due to the π-π* transition. The λ_{max} of TDPPTTB is blue shifted as compared to the corresponding TDPPTP (748 nm) and TDPPTT (826 nm).[12,13] Thus, the λ_{max} of the low energy absorption band is increasing in wavelength when shifting from ethynelene bond to phenyl and thiophene rings, respectively.

Passing from solution to the solid state the absorption spectrum of TDPPTTB becomes broader and the λ_{max} is 5 nm red shifted as compared to λ_{max} in solution with the appearance of a pronounced shoulder at around 800 nm. The red shift of 5 nm in λ_{max} of TDPPTTB is significantly lower as compared to TDPPTT (23 nm) and TDPPTP (13 nm).[12,13] The λ_{onset} of TDPPTTB is situated at 910 nm, corresponding to an optical band gap of 1.36 eV. The optical band gaps of TDPPTP and TDPPTT are 1.53 eV and 1.30 eV, respectively. Therefore, the ethynelene bond fine tunes the optical band gap of DPP-based copolymers between the optical band gaps deduced when phenyl or thiophene rings are used.

The emission spectrum of TDPPTTB has also been recorded in the solid state (Fig. 2). TDPPTTB exhibits photoluminescence in the near infrared (NIR) spectrum with an emission maximum at 878 nm and a pronounced shoulder at 933 nm. This implies that TDPPTTB, in mixtures with suitable electron acceptor materials, can be a suitable candidate for applications in NIR photodetectors. Further studies on the electroluminescence properties of TDPPTTB are underway.

Figure 2

Electrochemical Properties

The oxidation and reduction potentials of TDPPTTB have been determined by cyclic voltammetry measurements in *o*-DCB to lie at 0.11 V and −1.47 V vs. Fc/Fc^+ (the cyclic voltammograph is presented in the SI), resulting in estimated HOMO and LUMO energy levels of − 5.21 and− 3.63 eV vs. vacuum as derived from the equations $E_{HOMO} = -5.1 + E_{onset}^{oxid}$ (eV) and $E_{LUMO} = -5.1 + E_{onset}^{red}$ eV, respectively (Figure 3). The electrochemical bandgap, E_g^{CV} = 1.58 eV, is slightly higher than the optical bandgap (E_g^{opt} = 1.36 eV). Moreover, TDPPTT exhibits a HOMO at −5.17 eV and LUMO at −3.61 eV vs. vacuum (oxidation and reduction potentials in o-DCB lie at 0.07 V and −1.49 V vs. Fc/Fc^+),[12] whereas TDPPTP demonstrates a HOMO at −5.35 eV and LUMO at − 3.53 eV vs. vacuum (oxidation and reduction potentials in *o*-DCB lie at 0.25 V and −1.57 V vs. Fc/Fc^+).[13] Therefore, it is evident that ethynylene moiety drives the LUMO level towards deeper values (stronger electron affinity) as compared to thiophene and phenyl rings in DPP-based copolymers, while the HOMO level is fixed between the HOMO levels of TDPPTP and TDPPTT, respectively (Fig. 3), indicating that the ethynylene moiety is decreasing the donor character of thiophenes that flank the DPP.

The density functional theory calculations using the B3LYP/6-31G(d,p) performed on the tetramer model compounds of TDPPTB, TDPPTT, and TDPPTP (Fig. 3) provide an estimation of the HOMO, LUMO, and band gap energies. There is an excellent trend between the theoretical and experimental LUMO levels as well as on the electrochemical band gap with the theoretical prediction for the DPP-based copolymers. On the other hand, while the trend between the experimental and theoretical HOMO levels of TDPPTT and TDPPTP are in good agreement, there is a minor discrepancy on the HOMO level of TDPPTTB. The experimental HOMO level of TDPPTTB shows that it is situated between the HOMO levels of TDPPTT and TDPPTP while the calculation shows that the HOMO level is situated at deeper values as compared to TDPPTT and TDPPTP.

Figure 3

Morphological Properties

The topography and phase images recorded from AFM measurements of TDPPTTB film on a glass substrate annealed at 100, 120, 140, and 160°C are displayed in Fig. 4. At 100°C, the film shows the typical appearance of possibly an amorphous polymer film in this case with small aggregated features. Similar morphology has been reported in the case of TDPPTT film also annealed at 100°C.[14] As the annealing temperature increases, the film becomes more granular possibly due to more aggregation, particularly after 120°C where the film shows more distinct granules. All the changes in the topography images are also reflected in the phase images.

Figure 4

Charge Transporting Properties in Field-effect Transistors

Transistors based on TDPPTTB were first fabricated using the BG-BC architecture as shown in Fig. 5(a). The transfer characteristics of the representative device (W = 10 mm and L = 20 μm) measured after each annealing temperature are displayed in Fig. 5(b). All transistors show ambipolar characteristics with hole transport (red lines) at negative voltages (both drain voltage V_D and gate voltage V_G) and electron transport (blue lines) at positive voltages. Initially after annealed at 100°C, the holes show on-to-off current ratio ($I_{on\text{-}off}$) of approximately 5×10^4 while the electrons display $I_{on\text{-}off}$ of 10^4. The average linear mobilities (μ_{lin}) for holes and electrons are 0.002 $cm^2\ V^{-1}\ s^{-1}$. The average saturation mobilities (μ_{sat}) are higher, i.e., at 0.05 $cm^2\ V^{-1}\ s^{-1}$ for holes and 0.02 $cm^2\ V^{-1}\ s^{-1}$ for electrons. The onset voltage (V_{on}) for holes is at -10 V and for electrons at 40 V. The trap density which is calculated from the subthreshold swing[26] are around $1.1\text{-}1.2\times10^{13}$ $cm^{-2}\ eV^{-1}$ for both holes and electrons. The next annealing temperature at 120°C leads to more balance characteristics between holes and electrons [Fig. 5(c)]. $I_{on\text{-}off}$ of holes becomes 2×10^4 while that of electrons remains at 10^4. V_{on} of holes and electrons are shifted to -16 V and 26 V, respectively. μ_{lin} of holes decreases to 0.001 $cm^2\ V^{-1}\ s^{-1}$ while that of electrons is little changed at 0.002 $cm^2\ V^{-1}\ s^{-1}$. Similarly, μ_{sat} of holes drops slightly to 0.03 $cm^2\ V^{-1}\ s^{-1}$ with μ_{sat} of electrons stays at 0.02 $cm^2\ V^{-1}\ s^{-1}$. D_{tr} for both types of carriers marginally increase to $1.2\text{-}1.3\times10^{13}$ $cm^{-2}\ eV^{-1}$. Further annealing at 140 °C sees additional
decrease in the mobilities of both carriers with μ_{lin} now in the range of 0.0005 to 0.001 $cm^2\ V^{-1}\ s^{-1}$ and μ_{sat} of approximately 0.01 $cm^2\ V^{-1}\ s^{-1}$. $I_{on\text{-}off}$, V_{on}, and D_{tr} are however relatively unchanged. Higher annealing at 160°C significantly reduces the performance of both hole and electron transport. $I_{on\text{-}off}$ drop to 10^3 while μ_{lin} and μ_{sat} decrease to 0.0003 $cm^2\ V^{-1}\ s^{-1}$ and 0.003 $cm^2\ V^{-1}\ s^{-1}$, respectively. V_{on} of holes is -23 V and of electrons is 36 V. Lastly, D_{tr} increase to $1.5\text{-}1.6\times10^{13}$ $cm^{-2}\ eV^{-1}$. Fig. 5(c) summarizes the changes of the performance metrics with the annealing temperature. The overall behaviour of diminishing performance with the increasing annealing temperature might be explained by the change in the morphology of the TDPPTTB film as shown in the previous section. More aggregation of the polymer at higher annealing temperatures can hinder charge transport as well as increases the traps at the semiconductor/dielectric interface; both cases are reflected correspondingly in the reduced carrier mobilities and increased D_{tr}.

Figure 5

Transistors employing the TG-BC architecture based on TDPPPTTB and either of the two dielectrics, Cytop and P(VDF-TrFE-CFE), were next fabricated and measured [Fig. 6(a)]. The annealing condition was chosen to be 120°C due to good performance and more balance hole and electron transport as seen from the results of BG-BC transistors. The representative transfer and output characteristics of Cytop-based devices are shown in Fig. 6(b). Ambipolar behaviour is also observed with electron transport dominating. $I_{on\text{-}off}$ of electrons is 10^5 while that of holes is 2×10^4. Mobilities of electrons are approximately 4-5 times larger than those of holes both in linear and saturation regimes. μ_{lin} of electrons and holes are 0.008 $cm^2\ V^{-1}\ s^{-1}$ and 0.002 $cm^2\ V^{-1}\ s^{-1}$, and μ_{sat} are 0.02 $cm^2\ V^{-1}\ s^{-1}$ and 0.004 $cm^2\ V^{-1}\ s^{-1}$, respectively. D_{tr} of both carriers are not drastically different however, i.e., 3.6×10^{12} and 4.5×10^{12} $cm^2\ V^{-1}\ s^{-1}$. We speculate that the difference between electron and hole transport is possibly due to deep trap states that are not assessable using D_{tr} which relies on the subthreshold characteristics of the transistors. Instead, these deep traps manifest themselves in the onset voltage. Indeed for these Cytop-based devices, V_{on} of electrons is 50 V while that of holes is around -120 V, suggesting that there are more deep hole traps than deep electron traps. Low-voltage operation is achieved by employing the high-k relaxor ferroelectric polymer P(VDF-TrFE-CFE) as the dielectric layer.[27] The geometric capacitance of P(VDF-TrFE-CFE) film used in this work was obtained from an impedance analysis measurement at 10 Hz and found to be 200 nF cm^{-2}. Fig. 6(c) shows the representative transfer and output characteristics of low-voltage TDPPTTB transistors. The ambipolar behaviour in this case is slightly dominated by hole transport. $I_{on\text{-}off}$ for both carriers are close to 10^3. Mobilities of holes are 3-4 times larger than those of electrons. μ_{lin} of electrons and holes are 0.0005 $cm^2\ V^{-1}\ s^{-1}$ and 0.002 $cm^2\ V^{-1}\ s^{-1}$, and μ_{sat} are 0.002 $cm^2\ V^{-1}\ s^{-1}$ and 0.005 $cm^2\ V^{-1}\ s^{-1}$, respectively. Again, the difference in the transport performance is not mirrored in the D_{tr} which are around $5.3\text{-}5.6\times10^{13}$ $cm^{-2}\ eV^{-1}$ for both carriers. Similar to the Cytop-based devices, the imbalance shows in V_{on} which is 7 V for electrons and -1.5 V for holes.

Figure 6

Fig. 7 summarizes and compares the performance in terms of carrier mobility among different dielectrics of TDPPTTB-based transistors. The details of the density of states in the semiconductor and/or at the semiconductor/dielectric interface are needed to understand comprehensively about the difference in the performance; however, this is out of the scope of this work and will be a subject of further studies. The mobilities obtained here especially in the case of HMDS-treated SiO_2 dielectric are comparable to values reported earlier for TDPPTP and TDPPTT transistors.[12,13] The introduction of the ethynylene moiety therefore enables the tuning of the energy levels of TDPPT-based polymers without adversely affecting the charge transport properties, hence find possible applications in different optoelectronic devices, including OFETs, OPVs and NIR photodetectors.

Figure 7

Conclusions

In principle, ethynylene linkage could be used as a tool to fine-tune the polymer band gaps and HOMO values, especially

for the design of new conjugated polymers for FETs and OPV applications. In addition, ethynylene moiety provide a synthetic route to copolymerize electron-withdrawing monomers in alternating fashion. We used the latter procedure to synthesize a new DPP-based copolymer with deep HOMO level and narrow band gaps. Charge transport study based on transistors also show that the similar carrier transport properties are retained when compared to TDPPTT and TDPPTP. For TDPPTTB films annealed at 120 °C, the average mobilities from HMDS-treated SiO_2-based transistors are 0.03 cm^2 V^{-1} s^{-1} and 0.02 cm^2 V^{-1} s^{-1} for holes and electrons, respectively.

Experimental

Measurements

^{1}H NMR spectrum was recorded on a Bruker Avance 500 machine at 400 MHz. Deuterated solvents were used for homonuclear lock and the signals are referenced to the deuterated solvent peaks. Molecular weights (M_n and M_w) were determined by gel permeation chromatography (GPC) (Ultrastyragel columns with 500 and 10^4 Å pore size; $CHCl_3$ (analytical grade) was filtered through a 0.2 μm Millipore filter; flow 1 mL min^{-1}; room temperature) using polystyrene standards for calibration.

The UV-Vis absorption spectra of TDPPTTB in chloroform solution (0.2 % w/v) and as thin film were measured with a LAMBDA 950 UV/VIS/NIR Spectrophotometer of Perkin Elmer with spectral range from 250 nm to 2500 nm. For the preparation of the film, the solution was drop casted on quartz substrate. After the evaporation of the solvent, the film was ready for study. For the PL spectra a thin layer of TDPPTTB was spin-coated onto a quartz substrate and placed into a vacuum chamber with optical access. For sample excitation a He−Cd CW laser operating at a wavelength of 325 nm, with 35 mW power is used. The PL spectra were measured at room temperature and resolved by using a UV grating and a sensitive, calibrated liquid nitrogen cooled CCD camera.

Fourier transform infrared (FT-IR) spectrum was measured on a BRUKER FT-IR spectrometer IFS 66v/F (MIR). The sample was in a powder form. In addition, the polymer was characterized by Raman spectroscopy at room temperature on a Nicolet Almega XR Raman spectrometer with a 473 nm blue laser as an excitation source. For the preparation of the samples, the solution was deposited on Si wafers.

CV studies were performed using a standard three-electrode cell. Platinum disk electrode was used as working electrode, platinum mesh as the counter-electrode and platinum wire as a reference electrode. Tetrabutylammonium hexafluorophosphate ($TBAPF_6$; 98%) was used as electrolyte and was recrystallized three times from acetone and was dried in a vacuum at 100 °C before each experiment. Measurements were recorded using an EG&G Princeton Applied Research potensiostat/galvanostat Model 2273A connected to a personal computer running PowerSuite software. In a typical experiment, 2-5mg of the material was diluted in 0.1 M $TBAPF_6$ solution in *o*-DCB at a potential scan rate of 100 mV s^{-1}. The reduction potentials were calibrated against a ferrocene/ferrocenium (Fc/Fc^+) redox couple.

All calculations of the model compounds studied in this work have been performed using the Gaussian 03 software package.[28] The alkyl substituents have been replaced with methyl groups in the model compounds for our calculations. While the presence of these long alkyl chains enhances the solubility of these polymers and affect the charge carrier mobility and photovoltaic behaviour of the polymer,[29-31] from a computational point of view their replacement with shorter chains does not affect their optoelectronic properties (HOMO, LUMO and band gap) and thus the optimized structures of the molecules.[32] The ground-state geometry of each model compound has been determined by a full geometry optimization of its structural parameters using the density function theory (DFT) upon energy minimization of all possible isomers. In this work, the DFT calculations were performed using the Becke's three-parameter hybrid functional, B3, with non-local correlation of Lee-Yang-Parr, LYP, abbreviated as B3LYP in conjunction with the 6-31G(d,p) split valence polarized basis set. All calculations were performed in vacuum. No symmetry constraints were imposed during the optimization process. The geometry optimizations have been performed with a tight threshold that corresponds to root mean square (rms) residual forces smaller than 10^{-5} au for the optimal geometry. The energy level of the HOMO and the LUMO of the repetitive units of each polymer were carried out by using the same set of calculations. DFT/B3LYP/6-31G(d,p) has been found[33] to be an accurate formalism for calculating the structural and electronic properties of many molecular systems. In our studies the theoretical calculations performed on the tetramer model compounds for DFT describe in good proximity the experimental band gaps, in a similar manner to recent studies in other molecular systems.[34,35]

Bottom-gate bottom-contact (BG-BC) transistors were fabricated using Si^{++}/SiO_2 (200 nm) substrate with ITO/Au (10 nm/30 nm) source/drain (S/D) electrodes pre-patterned with standard photolithography. The silicon substrate also served as a gate contact in this case. SiO_2 dielectric was treated with hexamethyldisilazane (HMDS) using vapour deposition at 80 °C for 30 min followed by thermal annealing also at 80 °C for another 30 min. TDPPTTB was spin-cast at 2000 rpm for 60 s from a 10 mg mL^{-1} solution in *o*-DCB which was kept stirring at 100 °C during the deposition. The film was annealed at 100 °C for 15 min before electrical characterization. The effects of thermal annealing were studied by annealing the samples further at 120, 140, and 160 °C for 15 min each time, and electrical characterization was performed after each annealing. Top-gate bottom-contact (TG-BC) transistors were fabricated on glass substrates with Al/Au (5 nm/25 nm) S/D contacts prepared by thermal evaporation through a shadow mask. TDPPTTB was spin-cast using the same procedure as the BG-BC FETs preparation but annealed at 120 °C for 15 min. The dielectric layer was then spin-cast on top of the semiconductor followed by a 40-nm-thick Al gate electrode also thermally evaporated through a shadow mask. Two types of dielectrics were used in this work: (1) Cytop (Asahi Glass), spin-cast at 2000 rpm for 60 s and annealed at 100 °C for 30 min and (2) high-*k* relaxor ferroelectric poly(vinylidene fluoride-trifluoroethylene-chlorofluoroethylene) [P(VDF-TrFE-CFE) at 56/36.5/7.5 mol%] for low-voltage operation,[27] spin-cast from a 30 mg mL^{-1} solution in 2-butanone at 3000 rpm for 30 s and annealed at 60°C for 3 h. All transistor fabrication steps were carried out in dry nitrogen atmosphere. Current-voltage characteristics of the transistors were acquired with an Agilent B2902A source/measure unit. The analysis of the data was based on the gradual channel approximation. All measurements were performed in a dry nitrogen atmosphere. Films of TDPPTTB were prepared on glass substrates following the same procedure used to fabricate transistors. Samples were annealed at 100, 120, 140, and 160 °C each for 15 min.

Topographic and phase images of TDPPTTB films were obtained using an Agilent 5500 atomic force microscope in tapping mode.

Synthetic procedure

1,2-bis(trimethylstannyl)ethyne was purchased from Sigma Aldrich and 3,6-bis(5-bromothiophen-2-yl)-2,5-bis(2-hexyl decyl)pyrrolo[3,4-*c*]pyrrole-1,4(2*H*,5*H*)-dione was purchased from Luminescence Technologies. Toluene (ACS grade) was distilled over sodium prior to use. All other chemicals were purchased from Aldrich and used without further purification.
Polymerization: In a toluene solution (71 mL) of 3,6-bis(5-bromothiophen-2-yl)-2,5-bis(2-hexyldecyl)pyrrolo[3,4*c*]pyrrole -1,4(2*H*,5*H*)-dione (0.645 g; 0.7109 mmol) and 1,2-bis(trimethylstannyl)ethyne (0.250 g; 0.7109 mmol) tetrakis(triphenylphosphine)-palladium(0) [$Pd(PPh_3)_4$] (16.5 mg) was added. The reaction mixture is stirred at 110 ^oC under an argon atmosphere for 12 h. The polymer is precipitated in a solution of methanol, filtered through thumble and washed on a Soxhlet apparatus with methanol, hexane, chloroform and chlorobenzene. The chloroform and chlorobenzene fractions are evaporated under reduced pressure, and the polymer is precipitated in methanol, filtered, and finally dried under high vacuum.

Acknowledgements

CLC would like to thank the Ministry of Education and Religious Affairs in Greece for the financial support of this work provided under the co-operational program "AdvePol: E850". The calculations in this study were performed at the Research Centre for Scientific Simulations (RCSS) at the University of Ioannina. P.P. is grateful to Cambridge Display Technology (CDT), UK and Anandamahidol Foundation, Thailand, for financial support. Dr Georgia Pagona is acknowledged for her help in the cyclic voltammetry experiments.

Notes and references

[a] Department of Physics and Centre for Plastic Electronics, Imperial College London, Exhibition Road, South Kensington, London SW7 2AZ, UK
[b] Institute of Electronic Structure and Laser (IESL), Foundation for Research and Technology-Hellas (FORTH), Heraklion, 71110 Crete, Greece
[c] Centre of Materials Technology & Photonics and Electrical Engineering Department, Technological Educational Institute (TEI) of Crete, Heraklion, 71004 Crete, Greece
[d] Department of Applied Physics and Materials Research Centre, The Hong Kong Polytechnic University, Hong Kong, China
[e] National Hellenic Research Foundation, 48 Vassileos Constantinou Avenue, Athens 11635, Greece
[f] Advent Technologies SA, Patras Science Park, Stadiou Street, Platani-Rio, 26504, Patra, Greece
Corresponding author Email: cchochos@advent-energy.com
† Electronic Supplementary Information (ESI) available: ^{1}H-NMR, FT-IR and Raman spectra, as well as the cyclic voltammograph of the synthesized polymer. Optimized co-ordinates of the monomer and tetramer model compounds after theoretical calculations. See DOI: 10.1039/b000000x/

1 A. J. Heeger, *Adv. Mater.*, 2014, **26**, 10.
2 M. Shahid, T. McCarthy-Ward, J. Labram, S. Rossbauer, E. B. Domingo, S. E. Watkins, N. Stingelin, T. D. Anthopoulos and M. Heeney, *Chem. Sci.*, 2012, **3**, 181.
3 P. Li, O. Fenwick, S. Yilmaz, D. Breusov, D. J. Caruana, S. Allard, U. Scherf and F. Cacialli, *Chem. Commun.*, 2011, **47**, 8820.
4 P. M. Beaujuge, S. Ellinger and J. R. Reynolds, *Nat. Mater.*, 2008, **7**, 795.
5 C. L. Chochos and S. A. Choulis, *Prog. Polym. Sci.*, 2011, **36**, 1326.
6 J. You, L. Dou, Z. Hong, G. Li and Y. Yang, *Prog. Polym. Sci.*, 2013, **38**, 1909.
7 C. L. Chochos, N. Tagmatarchis and V. G. Gregoriou, *RSC Adv.*, 2013, **3**, 7160
8 G. Li, R. Zhu and Y. Yang, *Nature Photon.*, 2012, **6**, 153.
9 J. Roncali *Macromol. Rapid Commun.*, 2007, **28**, 1761.
10 C. B. Nielsen, M. Turbiez and I. McCulloch, *Adv. Mater.*, 2013, **25**, 1859.
11 *WO*, 049695, 2005.
12 J. C. Bijleveld, A. P. Zoombelt, S. G. J. Mathijssen, M. M. Wienk, M. Turbiez, D. M. de Leeuw and R. A. J. Janssen, *J. Am. Chem. Soc.*, 2009, **131**, 16616.
13 J. C. Bijleveld, V. S. Gevaerts, D. Di Nuzzo, M. Turbiez, S. G. J. Mathijssen, D. M. de Leeuw, M. M. Wienk and R. A. J. Janssen, *Adv. Mater.*, 2010, **22**, E242.
14 J. S. Lee, S. K. Son, S. Song, H. Kim, D. R. Lee, K. Kim, M. J. Ko, D. H. Choi, B. S. Kim and J. H. Cho, *Chem Mater.*, 2012, **24**, 1316.
15 K. H. Hendriks, W. Li, G. H. L. Heintges, G. W. P. van Pruissen, M. M. Wienk and R. A. J. Janssen, *J. Am. Chem. Soc.*, 2014, **136**, 11128.
16 K. H. Hendriks, G. H. L. Heintges, V. S. Gevaerts, M. M. Wienk and R. A. J. Janssen, *Angew. Chem. Int. Ed.*, 2013, **52**, 8341.
17 X.-R. Zhang, L. J. Richter, D. M. DeLongchamp, R. J. Kline, M. R. Hammond, I. McCulloch, M. Heeney, R. S. Ashraf, J. N. Smith, T. D. Anthopoulos, B. Schroeder, Y. H. Geerts, D. A. Fischer and M. F. Toney, *J. Am. Chem. Soc.*, 2011, **133**, 15073.
18 Z. Chen, M. J. Lee, R. Shahid Ashraf, Y. Gu, S. Albert-Seifried, M. Meedom Nielsen, B. Schroeder, T. D. Anthopoulos, M. Heeney, I. McCulloch and H. Sirringhaus, *Adv. Mater.*, 2012, **24**, 647.
19 J. C. Bijleveld, B. P. Karsten, S. G. J. Mathijssen, M. M. Wienk, D. M. de Leeuw and R. A. J. Janssen, *J. Mater. Chem.*, 2011, **21**, 1600.
20 H.-W. Lin, W.-Y. Lee and W.-C. Chen, *J. Mater. Chem.*, 2012, **22**, 2120.
21 P. Sonar, S. P. Singh, Y. Li, Z.-E. Ooi, T.-J. Ha, I. Wong, M. S. Soh and A. Dodabalapur, *Energy Environ. Sci.*, 2011, **4**, 2288.
22 P.-T. Wu, F. S. Kim and S. A. Jenekhe, *Chem. Mater.* 2011, **23**, 4618.
23 W. Li, K. H. Hendriks, A. Furlan, W. S. C. Roelofs, M. M. Wienk and R. A. J. Janssen, *J. Am. Chem. Soc.*, 2013, **135**, 18942.
24 J. W. Jung, F. Liu, T. P. Russell and W. H. Jo, *Energy Environ. Sci.*, 2012, **5**, 6857.
25 B. Carsten, F. He, H. J. Son, T. Xu and L. Yu, *Chem Rev.*, 2011, **111**, 1493.
26 S. M. Sze and K. K. Ng, in Physics of Semiconductor Devices, John Wiley & Sons, 3rd edn., 2007, ch. 5, pp 243.
27 J. H. Li, Z. Sun and F. Yan, *Adv. Mater.*, 2012, **24**, 88.
28 M. J. Frisch, G. W. Trucks, H. B. Schlegel, G. E. Scuseria, M. A. Robb, J. R. Cheeseman, J. A. Montgomery, Jr., T. Vreven, K. N. Kudin, J. C. Burant, J. M. Millam, S. S. Iyengar, J. Tomasi, V. Barone, B. Mennucci, M. Cossi, G. Scalmani, N. Rega, G. A. Petersson, H. Nakatsuji, M. Hada, M. Ehara, K. Toyota, R. Fukuda, J. Hasegawa, M. Ishida, T. Nakajima, Y. Honda, O. Kitao, H. Nakai,

M. Klene, X. Li, J. E. Knox, H. P. Hratchian, J. B. Cross, V. Bakken, C. Adamo, J. Jaramillo, R. Gomperts, R. E. Stratmann, O. Yazyev, A. J. Austin, R. Cammi, C. Pomelli, J. W. Ochterski, P. Y. Ayala, K. Morokuma, G. A. Voth, P. Salvador, J. J. Dannenberg, V. G. Zakrzewski, S. Dapprich, A. D. Daniels, M. C. Strain, O. Farkas, D. K. Malick, A. D. Rabuck, K. Raghavachari, J. B. Foresman, J. V. Ortiz, Q. Cui, A. G. Baboul, S. Clifford, J. Cioslowski, B. B. Stefanov, G. Liu, A. Liashenko, P. Piskorz, I. Komaromi, R. L. Martin, D. J. Fox, T. Keith, M. A. Al-Laham, C. Y. Peng, A. Nanayakkara, M. Challacombe, P. M. W. Gill, B. Johnson, W. Chen, M. W. Wong, C. Gonzalez and J. A. Pople, GAUSSIAN 03, Revision E.01, Gaussian, Inc., Wallingford, CT, 2004.

29 L. Biniek, S. Fall, C. L. Chochos, D. V. Anokhin, D. A. Ivanov, N. Leclerc, P. Lévêque and T. Heiser, *Macromolecules*, 2010, **43**, 9779.

30 L. Biniek, S. Fall, C. L. Chochos, N. Leclerc, P. Lévêque and T. Heiser, *Org. Electron.*, 2012, **13**, 114.

31 L. Biniek, C. L. Chochos, N. Leclerc, O. Boyron, S. Fall, P. Lévêque and T. Heiser, *J. Polym. Sci. Part A: Polym. Chem.*, 2012, **50**, 1861.

32 C. L. Chochos, A. Avgeropoulos and E. Lidorikis, *J. Chem. Phys.*, 2013, **138**, 064901.

33 L. Pandey, C. Risko, J. E. Norton and J.-L. Brédas, *Macromolecules*, 2012, **45**, 6405.

34 J. Ku, Y. Lansac and Y. H. Jang, *J. Phys. Chem. C*, 2011, **115**, 21508.

35 L. E. Polander, L. Pandey, S. Barlow, S. P. Tiwari, C. Risko, B. Kippelen, J.-L. Brédas and S. R. Marder, *J. Phys. Chem. C*, 2011, **115**, 23149.

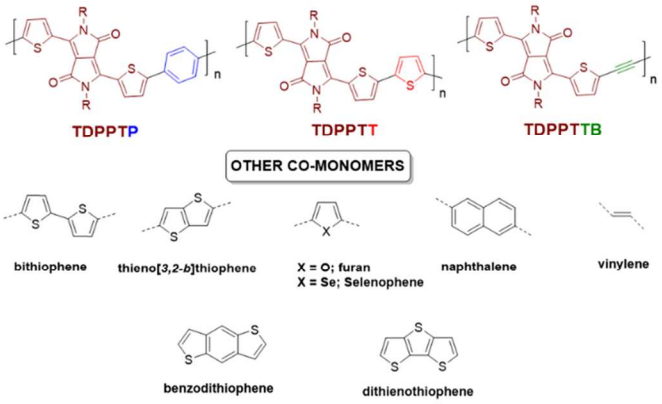

Scheme 1 Chemical structures of the various DPP alternating copolymers

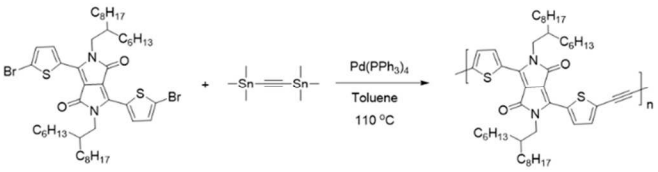

Scheme 2 Polymeric procedure towards the TDPPTTB

	θ1°	θ2°	θ3°
	8.60	9.93	24.97
	0.26	0.11	0.12
	0.00	0.00	0.00

Fig. 1 The results of the dihedral angles as calculated from the model compounds consisting of TDPPT unit and phenyl, thiophene and ethynylene groups

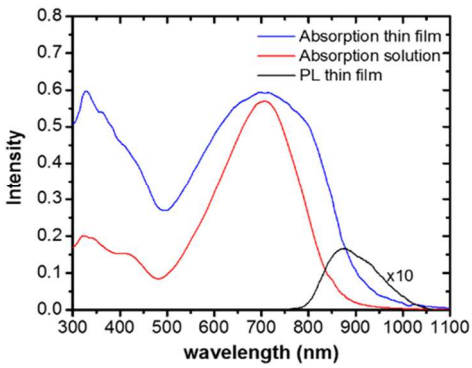

Fig. 2 Absorption spectra of TDPPTTB in chloroform solution and as thin film

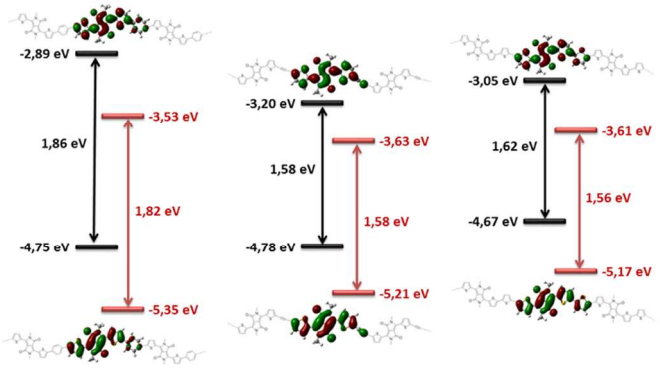

Fig. 3 Calculated HOMOs and LUMOs of the tetramer model compounds of the polymers using DFT at B3LYP/6-31(d,p) level of theory (black lines) and experimental energy levels obtained by cyclic voltammetry measurements (red lines) of TDPPTP (left), TDPPTB (center), and TDPPTT (right)

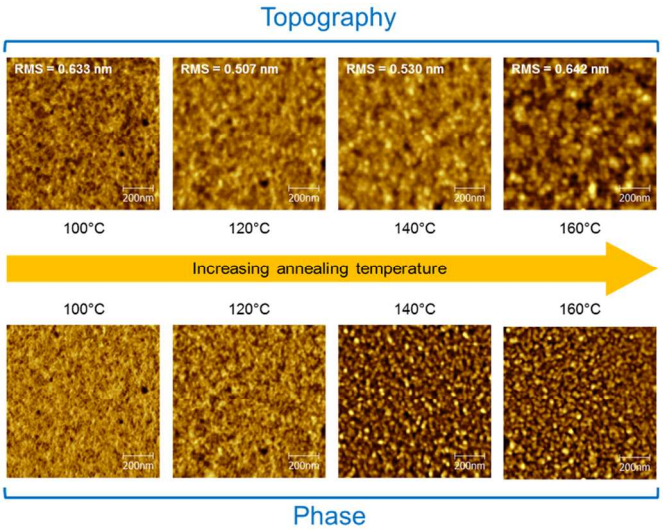

Fig. 4 AFM measurements showing topography and phase images of TDPPTTB film annealed at different temperatures. The scan size is 1 μm by 1 μm.

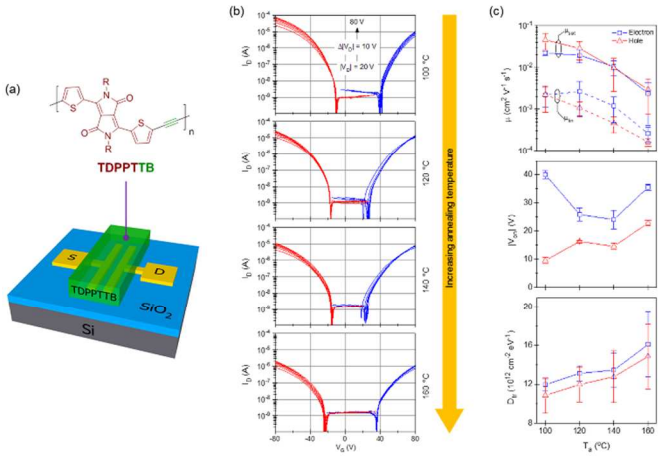

Fig. 5 (a) Schematic diagram of the bottom-gate bottom-contact (BG-BC) transistor. (b) Representative transfer characteristics of TDPPTTB-based BG-BC transistors annealed at different temperatures. Transistor dimensions are W = 10 mm and L = 20 μm. Red lines denote hole transport while blue lines denote electron transport. (c) Charge carrier mobility (μ), onset voltage (V_{on}), and trap density (D_{tr}) calculated from the transfer characteristics at each annealing temperature for both holes and electrons.

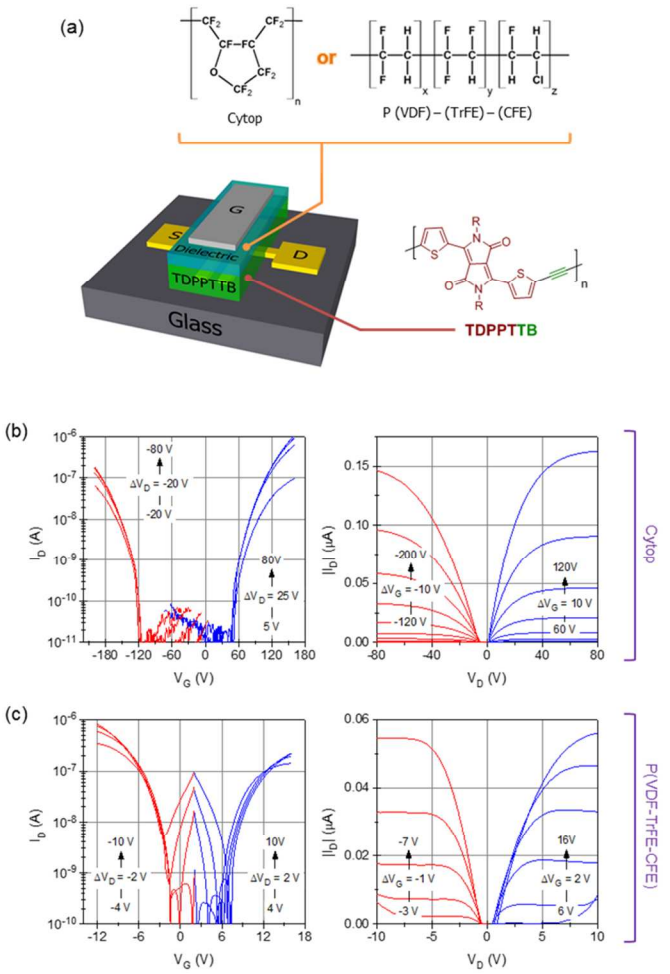

Fig. 6 (a) Schematic diagram of the top-gate bottom-contact (TG-BC) transistor and the molecular structures of Cytop and the high-k relaxor ferroelectric poly(vinylidene fluoride-trifluoroethylene-chlorofluoroethylene) [P(VDF-TrFE-CFE)] dielectrics. (b) Representative transfer (left) and output (right) characteristics of Cytop-based TDPPTTB TG-BC transistors. Device dimensions are W = 1 mm and L = 50 μm. (c) Similar to (b) but with P(VDF-TrFE-CFE) dielectric for low-voltage operation. Device dimensions are W = 1 mm and L = 20 μm. Red lines denote hole transport while blue lines denote electron transport.

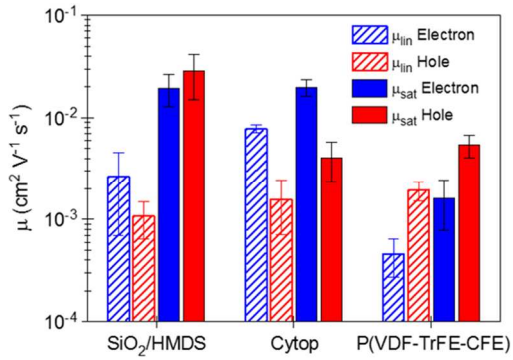

Fig. 7 Mobilities (μ) of TDPPTTB transistors based on different dielectrics. All values are calculated from 120 °C-annealed TDPPTTB films.

ToC Figure

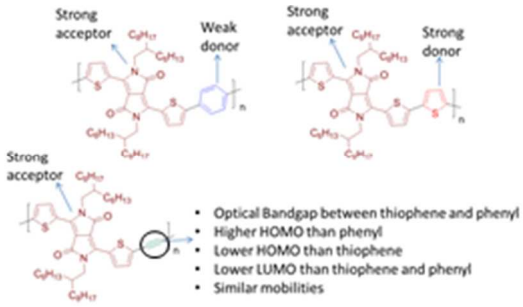

Adjasting the optoelectronic properties of conjugated copolymers by the introduction of ethynylene linkage